

RESEARCH PAPER

Green Silver Nanoparticles Synthesised by Medicinal plant *Echinops* sp. Root Extract for Antimicrobial Applications

H C Ananda Murthy

Department of Applied Chemistry, School of Applied Natural Science, Adama Science and Technology University, Adama, Ethiopia

ARTICLE INFO

Article History:

Received 19 July 2020

Accepted 28 September 2020

Published 15 October 2020

Keywords:

Green synthesis

Echinops sp.

Ag NPs

Antibacterial activity

Pathogens

ABSTRACT

Metallic nanoparticles have extraordinary antibacterial property. The silver NPs capped by biomolecules from medicinal plants can be disastrous to pathogens. For the first time, green silver nanoparticles (*EcS-Ag NPs*) were successfully synthesized from the Ethiopian medicinal plant *Echinops* sp. The most advanced techniques were employed to characterize the NPs. The presence of absorbance maxima, λ_{max} , at 454 nm confirms the formation of *EcS-Ag NPs*. The UV-DRS studies revealed the band gap of 2.22 eV for NPs. The role of biomolecules as capping agents for *EcS-Ag NPs* was authenticated by FT-IR spectra. The presence of 4 sharp peaks in the XRD pattern of NPs confirmed the highly crystalline nature of NPs. The purity of the NPs was corroborated by SEM-EDAX analysis. The mean particle length of NPs was found to be 33.86 nm. In addition, TEM micrographs revealed the presence of *EcS-Ag NPs* with varieties of nano-sized shapes. TEM-HRTEM-SAED analysis authenticated the presence of silver NPs with interplanar spacing value of 0.2418 nm which conformed to Ag (111) lattice fringes of NPs. The *EcS-Ag NPs* showed significant synergistic antibacterial effects against *S. aureus*, *E. coli*, *P. aeruginosa*, and *E. aerogenes*. The uppermost zone of inhibition of 18 mm was found against *S. aureus* bacteria. *EcS-Ag NPs* exhibited better antibacterial activities against gram-positive and gram-negative bacteria.

How to cite this article

Ananda Murthy H C. Green Silver Nanoparticles Synthesised by Medicinal plant *Echinops* sp. Root Extract for Antimicrobial Applications. *Nanochem Res*, 2020; 5(2):128-140. DOI: 10.22036/nrcr.2020.02.003

INTRODUCTION

The application of extracts of various medicinal plants as a traditional medicine for varieties of human's illnesses has been very common among many nations of the world since centuries. The vast majority of the rural people in the world completely rely on locally available plants with medicinal values. Ethiopia is one of the six centers of biodiversity in the world. Traditional medicine performs a tremendous role in Ethiopia, in which massive majority of Ethiopia's population lives in rural regions with little access to health offerings. In recent years, numerous Ethiopian medicinal plants have been validated in a scientific empirical

framework through phytochemical analysis and subsequent bioassays. It is understood that 25% of the modern medicines enters the market utilizing either directly or indirectly traditional medicinal plant parts. However, pharmaceutical manufactures use about 60% of these local plants. The medicinal plant species are used to treat number of diseases [1]. *Echinops* Sp., a 2nd ranked medicinal vegetation in Ethiopia, is valued primarily for its root parts and its medicinal uses are documented in the ancient medico-religious pharmacopoeia [2]. The roots of *Echinops* Sp., have been used in the preparation of medicines against migraine, mental illness, heart pain, leprosy, kidney disease, malaria and syphilis. It grows up to a height of 1.2 M with leafy stem. In

* Corresponding Author Email: anandkps350@gmail.com

order to explore the influence of biomolecules of medicinal plant on the eco-friendly synthesis of Ag NPs and to evaluate their cumulative antibacterial effect, *Echinops Sp.* plant has been chosen for our work.

The research on the fabrication of plant mediated Ag NPs for antimicrobial applications has gained significance in the recent years. The green Ag NPs have been used for photocatalytic, electrocatalytic, industrial dye degradation, nano medicinal, environmental and catalytic applications since many decades [3]. These Ag nanoparticles such as nanoparticles, nanocrystals, nanorods, nanotubes, and nanosheets exhibit versatile properties and hence found to exhibit inhibitory activity against many microorganisms and bacterial strains [4].

A very few medicinal plants such as *Azadirachta indica* [5], *Dioscorea bulbifera* [6], *Caesalpinia bonducella* [7], *Hagenia abyssinica* [8], *Mentha longifolia* [9], *Cocos nucifera* [10], *Syzygium cumini* [11], and Amazon Fruits [12] have been applied to synthesize silver, gold [13], copper and their oxides [14] in the recent past for multifunctional applications. The commonly adopted synthetic routes [15] for nanoparticles includes green synthesis [16], sol-gel synthesis [17], biosynthesis [18], microwave assisted solvent-free synthesis, micro emulsion method, etc.

Despite all advantages, no significant work has been performed on using medicinal plant root extracts to reduce and cap silver ions towards the synthesis of Ag NPs in Ethiopia for biomedical, photocatalytic, electrochemical sensor and antibacterial applications. Thus, the present work was attempted for the eco-friendly green synthesis of Ag NPs using medicinal plant *Echinops Sp.* plant root extract at low temperature to investigate synergistic influence of phytochemicals and Ag NPs on few selected bacterial strains. The synthesised Ag NPs have been characterised by all the advanced techniques and investigated for antibacterial properties.

EXPERIMENTAL

Chemicals and reagents

The chemical compounds and reagents, AgNO₃, C₂H₅OH, Mueller-Hinton agar solution, 0.5 McFarland standard, chloramphenicol discs, dimethyl sulfoxide, indigo carmine and malachite green dyes used during the experiments were of analytical grade (procured from Merck company).

Collection and authentication of plant materials

Echinops Sp. plant roots have been collected from the agricultural plots of Wondo Genet Agricultural Research Centre, Oromia, Ethiopia, after accomplishing the sector inspection. The authentication of *Echinops Sp.* (Code EB005) plant roots was conducted at Herbarium, Addis Ababa University.

Preparation of aqueous plant root extract

The roots of *Echinops Sp.* were washed repeatedly with water followed by rinsing with distilled water and then shade dried for 2 weeks to remove moisture content from the roots. The procedure followed is similar to the synthetic procedure reported in our earlier work [8] and thus not discussed in detail here. The prepared *Echinops Sp. plant root (EcS-PR) extract* was stored at 4 °C for future experiments.

Green synthesis of EcS-Ag NPs

100 mL of *EcS-PR* extract was mixed with AgNO₃ (400 mL of 0.5 M solution) in a 500 mL flask which was incubated for 24 hr at room temperature. The obtained brownish colored solution was centrifuged for 30 min at 8000 rpm to get black Ag NPs. These *EcS-Ag NPs* (Fig. 1) were washed, dried, ground and stored [19].

Characterization Techniques

X-ray diffractometer (Shimadzu-50 kV and 20 mA with Cu Ka radiation, $\lambda = 1.541 \text{ \AA}$) was used for crystal structure analysis. Chemical bonding interactions were explored using Shimadzu FTIR spectrophotometer (IR Affinity 1S). Shimadzu UV-visible spectrophotometer was utilized to evaluate the optical properties. Morphological analysis of the samples was conducted using JEOL, JEM-2100 (accelerating voltage up to 200 kV, LaB₆ filament) EDS-1.5 Å TEM resolution. The evaluation of interplanar spacings (IPS) of lattice fringes was done using Gatan Digital Micrograph software [15],[21].

Method of antimicrobial evaluation

All the antibacterial tests were conducted at Oromia Regional Laboratory, Adama, Ethiopia. Agar disc-diffusion method was adopted for the evaluation of *in-vitro* antibacterial properties of *EcS-Ag NPs* verses *S. aureus*, *E. coli*, *P. aeruginosa*, and *E. aerogenes*. The effectively growing bacterial



Fig. 1. The scheme of synthesis of EcS-Ag NPs.

cultures were dispersed on Mueller-Hinton Agar (MHA) plate (turbidity was adjusted with Tryptone Soy Broth, TSB to match 0.5 McFarland standard) The extract of the NPs was prepared with four different concentrations in Dimethyl Sulfoxide (DMSO). Four concentrations (6.25, 12.5, 25 and 50 $\mu\text{g}/\mu\text{l}$) of the synthesized NPs were added to the respectively labelled discs. The antibiotic discs of 6 mm diameter were applied to agar surface using forceps with gentle pressure and then impregnated with the dissolved extract. The positive and negative controls taken were chloramphenicol and DMSO, respectively. The plates were incubated at $35 \pm 2^\circ\text{C}$ in an ambient air incubator for 18-24 hours. The zone of inhibition was measured to the nearest millimeters (mm) using a ruler and recorded for all the samples.

RESULTS AND DISCUSSION

Synthesis of EcS-Ag NPs

The synthesis of EcS-Ag NPs was successfully performed using the EcS-PR extract to reduce and

cap silver ions to silver. The alkaloids, tannins, flavonoids and terpenoids were found in EcS-PR extract during the phytochemical analysis. The list of the phytochemicals present in the extract are as given in Table 1.

Three steps involved in the origin of NPs include: reduction of metal ions, formation of cluster and growth of nanoparticles. The biomolecules of the extract basically behave as antioxidants. In addition, the enzymes of EcS-PR extract also assist silver ions to get reduced and form protein capped silver NPs. It is worth noting that that phytochemicals act as the organic ligands assisting the reduction of silver ions to silver NPs. In addition, these compounds also influence the size of the nanoparticle as reported by the earlier researchers [22].

Characterization of EcS-Ag NPs

The EcS-Ag NPs were characterized by employing UV-visible, UV-DRS, FT-IR, XRD, SEM, EDXA, TEM, HRTEM and SAED techniques.

The UV-visible absorbance spectrum of

Table 1. The details of phytoconstituents screening of Echinops Sp. plant root extract.

Sl. No.	Phytoconstituents	Test / Reagent	Result
1	Alkaloids	Wagner's reagent	+
2	Tannins	KOH	+
3	Flavonoids	Shinoda Test	+
4	Terpenoids	Salkowski Test	+
5	Anthraquinone glycosides	Borntrager's Test	-
6	Cardiac glycosides	Keller-Kiliani Test	-
7	Saponins	Frothing Test	-

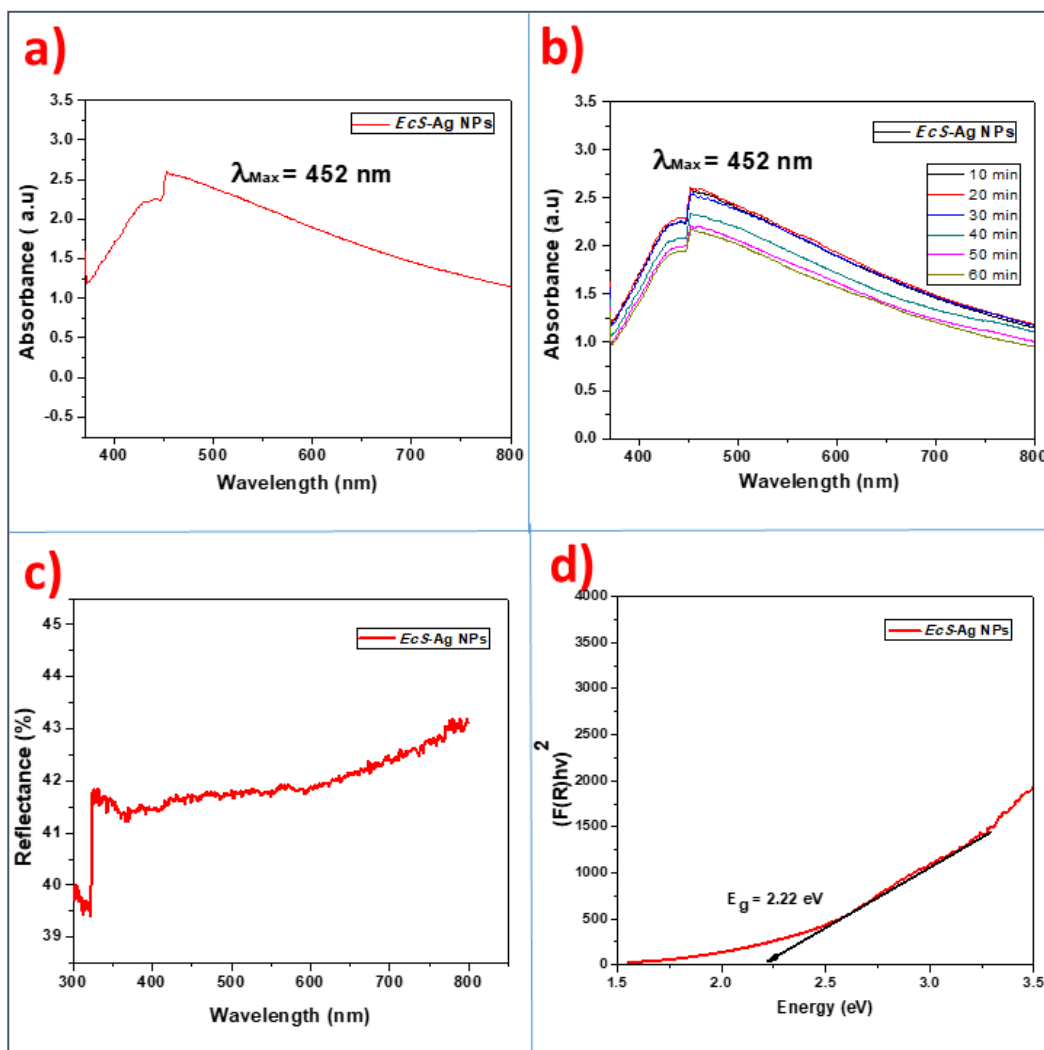


Fig. 2. (a) and (b) The absorbance spectrum of EcS-Ag NPs at different time intervals. (c) The UV-DRS spectrum of EcS-Ag NPs. (d) The Tauc plot of EcS-Ag NPs (yielding E_g value).

instantaneously synthesised EcS-Ag NPs revealed λ_{max} of 452 as shown in Fig. 2a, just after 10 min of mixing plant extract with silver nitrate solution. The absorbance spectrum recorded after 20, 30,

40, 50 and 60 minutes of forming homogeneous mixture exhibited identical absorbance bands at λ_{max} of 454 nm (Fig. 2b).

The enhanced absorbance in the consecutive

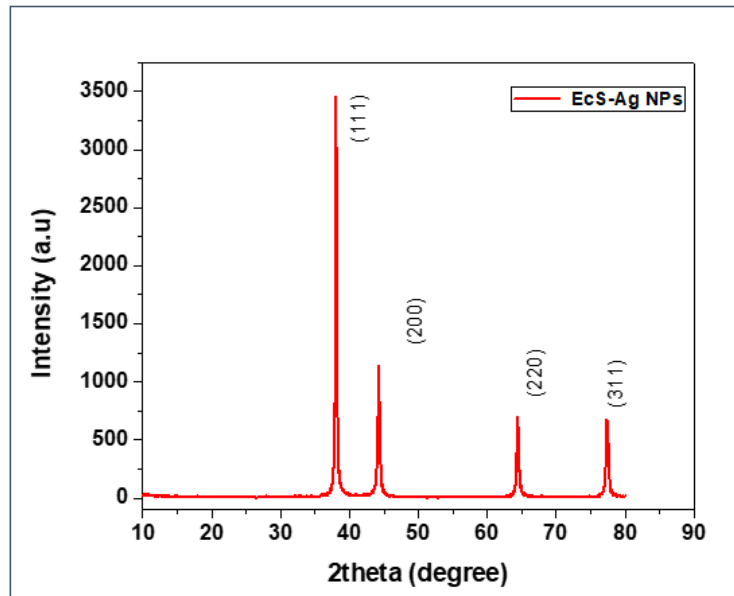


Fig. 3. The XRD pattern of EcS-Ag NPs.

bands clearly confirms the increased concentration of nanoparticles. As the time passes on, the reduction of silver ions is followed by nucleation of small cluster of silver atoms to form nanoparticles in the presence of biomolecules of plant extract that may act as a reducing and stabilising agent.

Almost identical results were observed during the analysis of the synthesized Ag NPs using the *Lustrum lucidum* leaf extract [23] and *Persea americana* seed extract [24]. The surface plasmon absorbance presents a set of different λ_{max} values for NPs synthesised using different plant extracts which is possibly due to morphological features of the NPs. The UV-Vis-DRS spectrum was recorded (Fig. 2c) for NPs. For the most part of the plot, the Kubelka - Munk capacity $F(R)$ is modified over the diffused reflectance into equivalent absorption coefficient and utilized for investigating the powders as given by equation (1),

$$F(R) = \frac{(1-R)^2}{2R} \quad (1)$$

where R is the reflectance, and $F(R)$ is Kubelka-Munk function. The optical energy gap was calculated using Tauc relation as in equation (2),

$$F(R) h\nu = A (h\nu - E_g)^n \quad (2)$$

where $n = 1/2$ and 2 are for direct and indirect transitions, respectively, for indirect band and

direct band [25]. The optical energy gap was calculated using Tauc relation as in equation (2) thereby giving direct band [26]. The Tauc plot (Fig. 2d) was utilized to compute the band gap energy of EcS-Ag NPs. The energy gap (E_g) of 2.22 eV was deduced for EcS-Ag NPs.

The XRD analysis was executed to explore the in-depth details of crystal structure of EcS-Ag NPs. The XRD spectrum of EcS-Ag NPs (Fig. 3) demonstrates a total of 4 prominent peaks. These peaks with 2θ values of 38.14°, 44.7°, and 64.50°, and 77.42° conform to 111, 200, 220 and 311 crystal lattice planes of silver (fcc structure) and the diffraction data is in compliance with the data of ICPD card No. 004-7383 (Fm3m) [27].

The average crystallite size (D) obtained for EcS-Ag NPs was deduced to be 21.47 nm respectively by using Scherrer's formula [28].

$$D = K\lambda / \beta \cos\theta \quad (3)$$

where, K is a constant, λ is wavelength of X-rays and β is full width at half maximum (FWHM).

The FTIR spectroscopy was helpful in revealing the bonding features of both EcS-PL extract and EcS-Ag NPs. The intense peaks, shown in Fig. 4, at 3395 cm^{-1} correspond to -OH stretching frequencies. The peak at 1718 cm^{-1} arises due to C=O vibration of ketonic groups. The small peak at 2925 cm^{-1} was correlated to the alkane C-H stretching mode. The

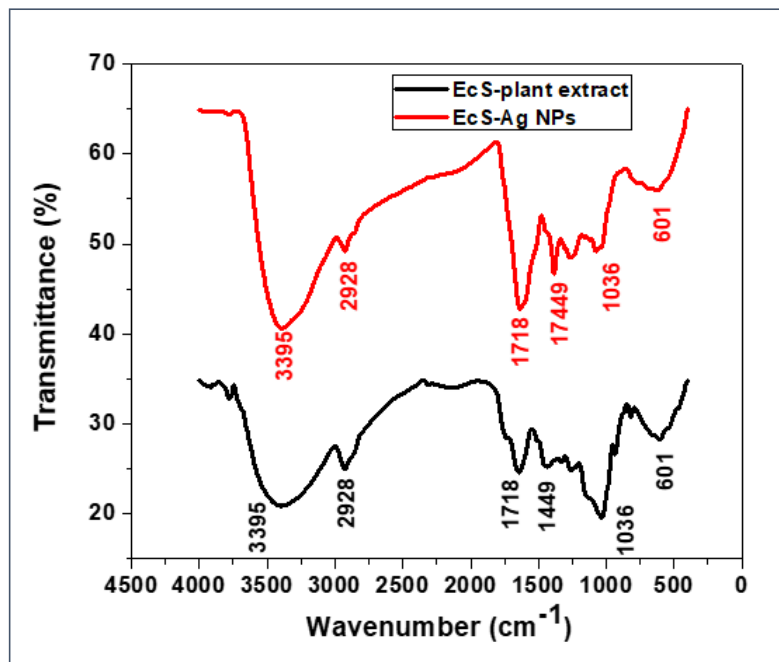


Fig. 4. The FTIR spectra of EcS plant extract and EcS-Ag NPs

vibration of $-\text{COO}$ group of carboxylic acid was found to appear at 1449 cm^{-1} . A moderately intense band at around 1035 cm^{-1} confirms the stretching of C-O-C bond. The presence of prominent peaks at 3395 cm^{-1} , 1718 cm^{-1} , 1449 cm^{-1} , 1035 cm^{-1} and 601 cm^{-1} in the FTIR spectra of both plant root extract and NPs clearly indicate the presence of bioactive molecules around the NPs. These bioactive molecules have shown a sizable function in the nucleation and growth of EcS-Ag NPs. The bending vibrations of Ag-O-H bonds resulted in a small peak at 601 cm^{-1} , possibly due to Ag-O bond. The FTIR spectral inspection confirmed the presence of phytochemicals (phenolics, tannins, glycosides and proteins) in EcS-PR extract and their roles as a reducing and stabilizing agent during the synthesis of EcS-Ag NPs. Especially the phenolics were reported to be strong candidates for binding with silver NPs [29].

The electron microscopy was applied to investigate the morphological features of EcS-Ag NPs. The SEM micrographs of NPs in Fig. 5a-b depict varieties of nanoparticles with diverse shapes and sizes.

The presence of mixed type of NPs is possibly due to the nature and amount of capping agents around the particles. The average grain size of Ag NPs was found to be in the range of 5–50 nm [30].

The presence of less agglomerated Ag NPs due to high surface area yielded small size particles. The Ag NPs were found to be as small as 6.5 nm, clearly confirming the efficient role of biomolecules as stabilizing agents preventing the growth of silver clusters to bigger NPs.

The EDAX analysis revealed the elemental composition of the EcS-Ag NPs as depicted in Fig. 5c. The elements, Ag, C, O, Si, S and Cl have been identified in the spectrum and additional peaks appeared due to the usage of standard during the analysis as well as impurities.

In order to gain deep insight about the shape, size and structure of the EcS-Ag NPs, TEM-HRTEM-SAED technical micrographs and patterns have been well utilized [31]. As shown in Fig. 6a-d, the HRTEM images (at different magnifications) affirm that as-synthesized EcS-Ag NPs are mostly spherical, regular as well as irregular in geometry. This is possibly due to the dual role (reducing and stabilizing) played by the bioactive molecules of EcS-PL extract.

The existence of nanosized particles (6.5 nm) approves the efficient role of bioactive components of the extract as capping and stabilizing agents, otherwise agglomerated particles are formed.

The TEM images of EcS-Ag NPs are depicted in Fig. 6a-d. A mixture of diversely shaped particles

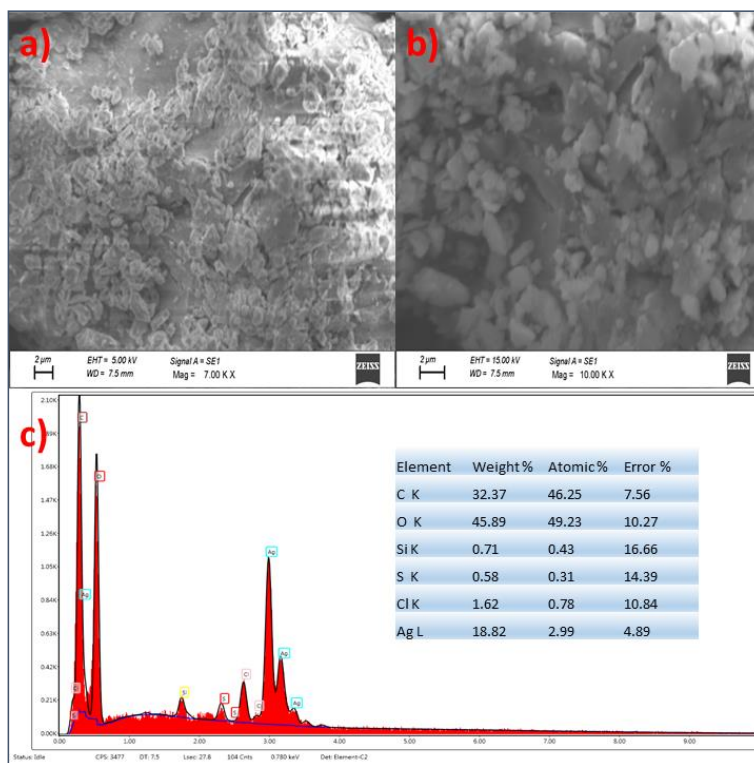


Fig. 5. (a), (b) and (c) The SEM micrographs of EcS-Ag NPs. (d) The EDAX spectrum of EcS-Ag NPs.

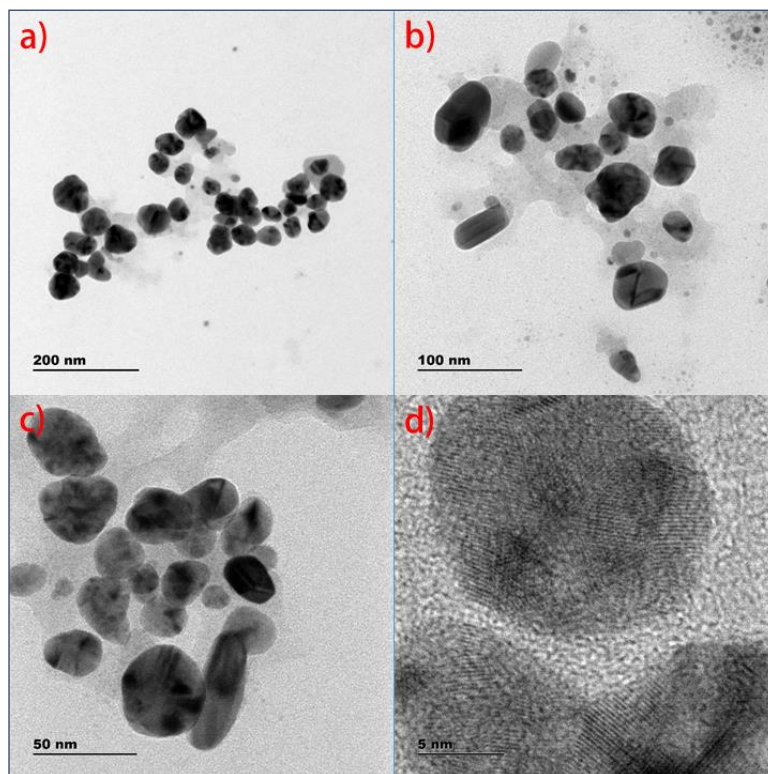


Fig. 6. The TEM images of EcS-Ag NPs with nearly spherical shapes at various magnifications a) 200 nm, b) 100 nm, c) 50 nm, and d) 5 nm.

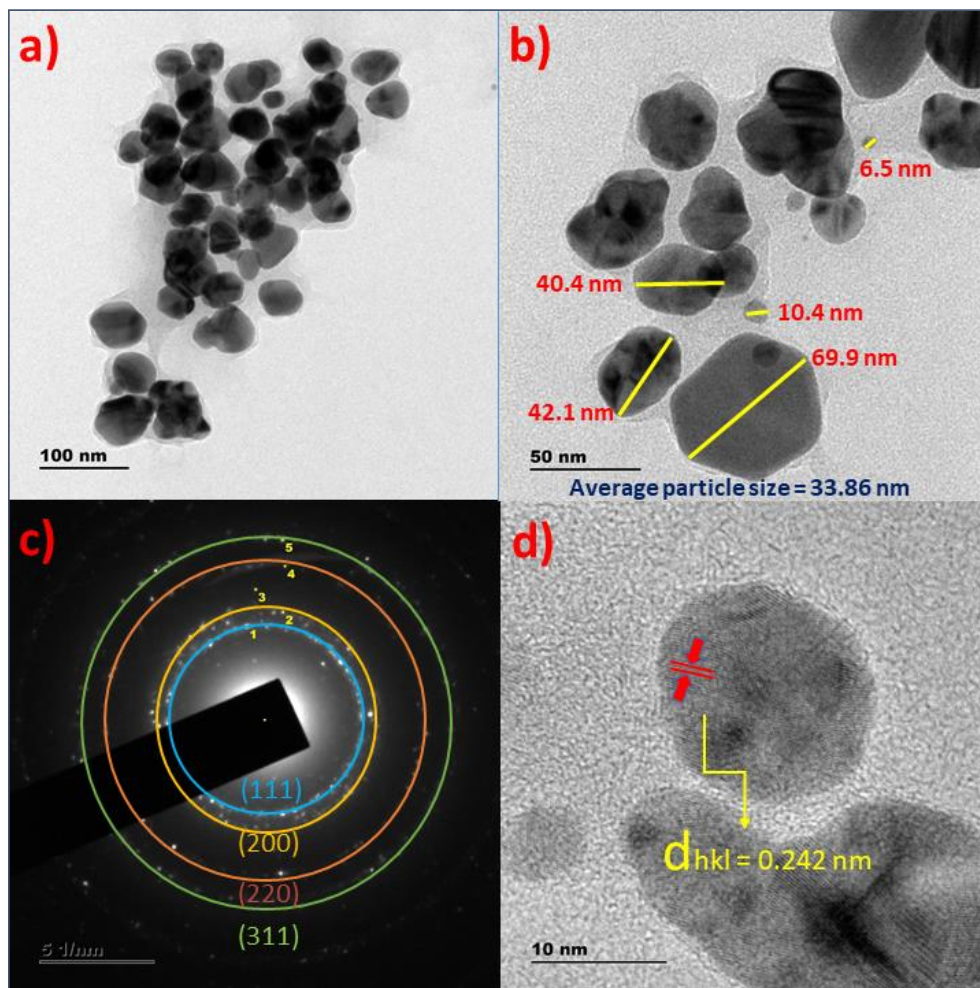


Fig. 7. The TEM micrographs of EcS-Ag NPs at (a) weak magnification (100 nm) and (b) strong magnification (50 nm). (c) The SAED pattern (6 spots), and (d) The HRTEM micrographs of lattice fringes of EcS-Ag NPs with IPS value of 0.242 nm.

including cylindrical, hexagonal, and triangular shapes were found in these images. It is worth to note that the particle size and shape control still remains a great challenge as no external constraints were imposed during the experimentation. This result, indicating the formation of various sizes and shapes, is in close agreement with the earlier findings [32]. The spherical structures with various sizes ranging from 6.5 nm to 42.1 nm with the average size of 33.86 nm are shown in Fig. 7a-b.

The five spots appeared on the SAED pattern were correlated to specific crystal planes of EcS-Ag NPs as shown in Fig. 7. The most prominent 4 spots shown in colored concentric circles represent (111), (200), (220) and (311) planes. The interplanar spacing (IPS) value of 0.242 nm for Ag (111) plane is deduced from Fig. 7d. Figs. 8a, 8b

and 8c respectively show the HRTEM micrographs of EcS-Ag NPs with enhanced lattice fringes, IFFT, and profile of IFFT with interplanar spacing (IPS) value for a specified plane. The IPS values for a specific parallel crystal planes on the surface of Ag NPs were found to be 0.2418 nm at a specific point.

Table 2 provides the IPS values for the 5 spots appeared on the SAED pattern (Fig. 7c) of EcS-Ag NPs. Each spot on the SAED pattern corresponds to a specific set of lattice planes. The IPS values of 0.2417 nm, 0.2056 nm, 0.1471 nm, 0.2040 nm and 0.1254 nm, derived for spots 1, 3, 4 and 5, correspond to crystal planes 111(Ag), 200(Ag), 220(Ag) and 311(Ag) that are in accordance with the IPS values of Ag crystal structure [33]. The presence of other one spot (2) is possibly due to trace amount of crystalline AgCl. The presence of

Table 2. The interplanar spacing values for EcS-Ag NPs from SAED pattern.

Spot No.	Interplanar spacing (nm)	Rec. Pos. (1/nm)	Degrees to Spot 1	Degrees to x- axis	Amplitude
1	0.2417	4.137	0.00	80.37	2839.10
2	0.2141	4.671	2.04	78.33	4168.58
3	0.2056	4.865	52.10	28.27	4484.95
4	0.1471	6.796	6.11	74.26	1295.65
5	0.1254	7.974	5.87	86.24	5564.48

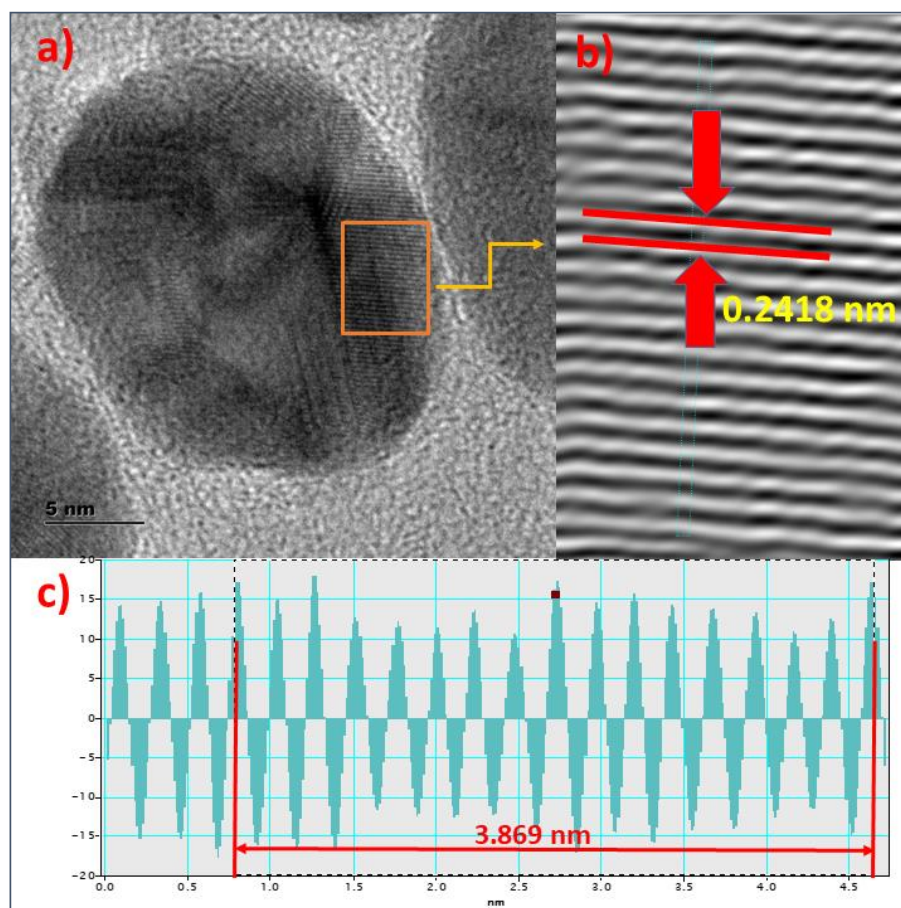


Fig. 8. The HRTEM morphology of EcS-Ag NPs. (a) Magnified lattice fringes, (b) IFFT patterns, and (c) profile of IFFT with d-spacing distance.

Cl peak in the EDAX spectrum of Ag NPs further confirms the possibility of AgCl formation.

This SAED analysis using HRTEM images is in compliance with the previously discussed XRD results for the EcS-Ag NPs [34]. The IPS value of lattice fringes at the surface of the EcS-Ag NPs was found to be 0.2418 nm, that is similar to the d_{hkl} value of 0.24 nm for (111) plane of fcc structured Ag obtained in the previously reported work [35].

Antimicrobial activity

The EcS-Ag NPs demonstrated superior antibacterial activities versus all the tested pathogens; *S. aureus*, *E. coli*, *P. aeruginosa*, and *E. aerogenes*. The present work evaluated synergistic influence of biomolecules with NPs against all these 4 pathogens. The zone of inhibitions (ZoI) for chloramphenicol, DMSO and NPs with four concentrations (6.25, 12.5, 25 and 50 $\mu\text{g}/\mu\text{l}$) are

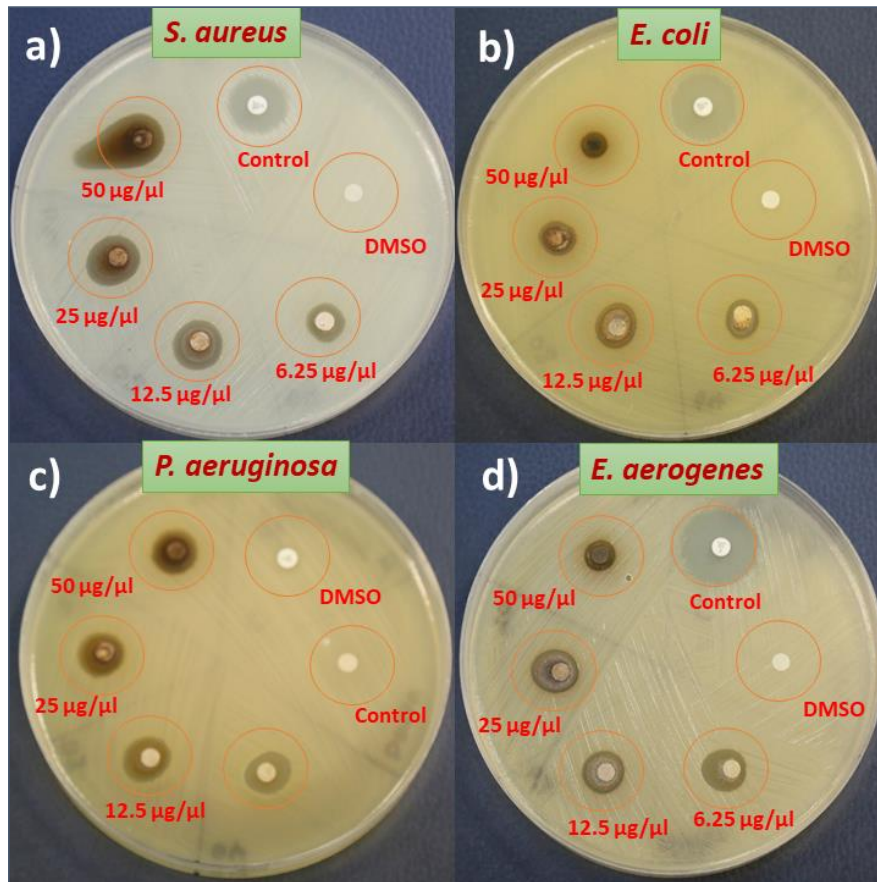


Fig. 9. The antibacterial activity of EcS-Ag NPs versus bacteria, S. aureus (b) E. coli (c) P. aeruginosa (d) E. aerogenes

Table 3. The zone of inhibitions for various bacteria by EcS-Ag NPs.

Concentration of NPs (µg/µl)	Bacterial strains and Zone of Inhibition in mm			
	<i>S. aureus</i> ATCC25923	<i>E. coli</i> ATCC25992	<i>P. aeruginosa</i> ATCC27853	<i>E. Aerogenes</i> ATCC13048
50	18	9	16	11
25	18	13	15	12
12.5	16	14	16	13
6.25	14	11	15	15
DMSO	6	6	6	6
Chloramphenicol	25	24	6	30

shown in Fig. 9. EcS-Ag NPs were found to show better antimicrobial activity against gram-negative bacterial strain E. aerogenes than the other gram-positive bacterial strains that could be attributed to the structural differences in the cell walls of bacteria [26].

The antimicrobial activity of NPs was highly appreciable against *S. aureus* with ZoI of 18 mm.

The maximum zone of inhibitions (mm) inscribed by EcS-Ag NPs against *E. coli*, *P. Aeruginosa* and *E. aerogenes* bacteria are 14 mm, 16 mm and 15 mm, respectively (Table 3). In addition, the lowest zone of inhibition was exhibited by *E. coli* bacteria remained at 9 mm for the most concentrated solution of NPs. In addition, two gram-negative bacteria *E. coli* and *E. aerogenes* exhibited the

Table 4. Comparative statistics of antimicrobial activities of Ag NPs synthesized by using various plant extracts.

Sl. No.	Plant extract	Zone of Inhibition (mm)	Tested Pathogens	Reference
1	Bergenia ciliata	8.5	S. aureus	[40]
2	Balloon flower plants	12	E. coli	[41]
3	Aloe fleurentiniorum	12, 14.5	E. coli, S. aureus	[42]
4	Chenopodium murale	12.7	S. aureus	[43]
5	Ocimum Sanctum (Tulsi)	14	E.coli	[44]
6	Acanthospermum hispidum	15, 16	E. coli, P. aurognosa,	[45]
7	Banana peel extract	17, 16, 12	E. coli, S. aureus, B. subtilis.	[46]
8	Echinops sp.	18, 14, 16, 15	S. aureus, E. coli, P. aurognosa, E. Aerogenes	Present work
9	Rosmarinus officinali	17.2, 18.8, 31.2, 16.2	E. coli, P. aurognosa, S. aureus, B. subtilis.	[47]
10	Citrus paradisi (grapefruit red)	22	E.coli	[48]
11	Coffea arabica	23, 21	E. coli, S. aureus	[33]

opposite trend of decreased antibacterial activity with increase in the concentrations of Ag NPs as against gram-positive bacteria. In the case of *E. coli*, the ZoI decreased from 14 mm to 9 mm on moving from 12.5 µg/µl to 50 µg/µl concentration. But gram-positive bacteria *S. Aureus* exhibited the opposite trend, where antibacterial activity increased with an increase in the concentration of A NPs. This behaviour is basically due to the structural differences between two types of bacteria as well as differences in the morphological features of Ag NPs.

The antimicrobial resistance recorded for *EcS-Ag* NPs was found to be superior when compared with few of the earlier results (Table 4) presented by many researchers, even though few other workers reported higher inhibitions that is believed to be due to the usage of higher concentrations of NPs or presence of higher concentrations of bioactive compounds. The highest zone of inhibition (mm) recorded with Ag NPs against bacteria was 18 mm. Thus, it can be concluded that the cumulative effect of Ag NPs coupled with phytochemicals (alkaloids, tannins, flavonoids and terpenoids) of *EcS-PR* extract proved to be detrimental for bacterial strains.

Even though many antimicrobial mechanisms were proposed by earlier researchers, the action of *EcS-Ag* NPs on the bacteria is unknown and yet to be exploited completely. Nanoparticles were found to cause the death of bacteria adopting direct or indirect ways by attacking bacteria's cell wall,

inhibiting RNA synthesis and preventing DNA replication. It is assumed that the positive Ag^+ in the NPs adsorb directly onto the cell wall of bacteria interacting with negatively charged species. This result in disruption of the cell wall of bacteria and via the generation of reactive oxygen species (ROS) by the effect of visible/UV light radiation [21]. It is also assumed that the cumulative effect of *EcS-Ag* NPs and bioactive compounds of *EcS-PL* extract displayed magnificent influence on bacteria as suggested by the recent studies [36].

The mechanism of NPs action basically differs as there exist significant structural differences between gram-negative and gram-positive bacteria [37]. In addition, electrochemical charge variations across the cell membrane influence the interactions with the released Ag^+ ions by *EcS-Ag* NPs deteriorating the structural integrity of the membrane [38]. The maximum antibacterial activity was recorded for gram-positive bacteria compared to the gram-negative bacteria due to their differences in their cell structures as well as the potentiality of nanoparticles. [39].

CONCLUSION

The application of medicinal plant *Echinops sp.* root extract towards the green synthesis of silver (*EcS-Ag*) nanoparticles was successful. The UV-visible spectra, XRD pattern, and FTIR spectra approved the formation of crystalline *EcS-Ag* NPs in the presence of biomolecules (alkaloids, tannins, flavonoids and terpenoids) of *EcS-PL* extract.

SEM-TEM-HRTEM-SAED analyses corroborated the existence of silver by the observation of Ag (111), (200), (220) and (311) lattice fringes in *EcS*-Ag NPs with the calculated interplanar spacing values matching exactly with the standard value for Ag. The synergistic influence of bioactive compounds and *EcS*-Ag NPs proved to exhibit highly effective antibacterial mechanism against pathogens, *S. aureus*, *E. coli*, *P. aeruginosa*, and *E. aerogenes* with the highest inhibition zone of 18 mm. It can be concluded that the cumulative effect of biomolecules of plant and silver NPs can be detrimental to disease causing pathogens.

ACKNOWLEDGEMENT

The author would like to thank the staff, Department of chemistry and Management of Adama Science and Technology University, Ethiopia for allowing me to use their facilities. This work has been funded through the project (ANSD/04/0453/11-2018) approved by Research and Technology Transfer Office, sanctioned by Adama Science and Technology University, Ethiopia.

CONFLICT OF INTEREST

The author declares that there is no conflict of interest.

REFERENCES

- Judžientienė A. Wormwood (*Artemisia absinthium* L.) Oils. *Essential Oils in Food Preservation, Flavor and Safety*: Elsevier; 2016. p. 849-56.
- Abera B. Medicinal plants used in traditional medicine by Oromo people, Ghimbi District, Southwest Ethiopia. *Journal of Ethnobiology and Ethnomedicine*. 2014;10(1):40.
- Egbe J, Ewa D, Ubi S, Ikwa G. Systemic Modeling of Soil Structure Dynamics for Civil Engineering Works in Calabar South.
- Hemmati S, Harris MT, Barkey DP. Polyol Silver Nanowire Synthesis and the Outlook for a Green Process. *Journal of Nanomaterials*. 2020;2020:1-25.
- Rajput N. Methods of preparation of nanoparticles-a review. *International Journal of Advances in Engineering & Technology*. 2015;7(6):1806.
- Ghosh S, Jagtap S, More P, Shete UJ, Maheshwari NO, Rao SJ, et al. Mediated Synthesis of Novel AucoreAgshell Nanoparticles with Potent Antibiofilm and Antileishmanial Activity. *Journal of Nanomaterials*. 2015;2015:562938.
- Sukumar S, Rudrasenan A, Padmanabhan Nambiar D. Green-Synthesized Rice-Shaped Copper Oxide Nanoparticles Using *Caesalpinia bonducella* Seed Extract and Their Applications. *ACS Omega*. 2020;5(2):1040-51.
- Murthy HCA, Desalegn T, Kassa M, Abebe B, Assefa T. Synthesis of Green Copper Nanoparticles Using Medicinal Plant *Hagenia abyssinica* (Brace) JF. Gmel. Leaf Extract: Antimicrobial Properties. *Journal of Nanomaterials*. 2020;2020:1-12.
- Javed B, Nadhman A, Mashwani Z-u-R. Phytosynthesis of Ag nanoparticles from *Mentha longifolia*: their structural evaluation and therapeutic potential against HCT116 colon cancer, Leishmanial and bacterial cells. *Applied Nanoscience*. 2020;10(9):3503-15.
- Uddin AKMR, Siddique MAB, Rahman F, Ullah AKMA, Khan R. Cocos nucifera Leaf Extract Mediated Green Synthesis of Silver Nanoparticles for Enhanced Antibacterial Activity. *Journal of Inorganic and Organometallic Polymers and Materials*. 2020;30(9):3305-16.
- Mittal D, Narang K, Leekha Kapinder A, Kumar K, Verma AK. Elucidation of Biological Activity of Silver Based Nanoparticles Using Plant Constituents of *Syzygium cumini*. *International Journal of Nanoscience and Nanotechnology*. 2019;15(3):189-98.
- Lima AKO, Vasconcelos AA, Sousa Júnior JVV, Escher SKS, Nakazato G, Taube Júnior PS. Green Synthesis of Silver Nanoparticles Using Amazon Fruits. *International Journal of Nanoscience and Nanotechnology*. 2019;15(3):179-88.
- Bansal SA, Kumar V, Karimi J, Singh AP, Kumar S. Role of gold nanoparticles in advanced biomedical applications. *Nanoscale Advances*. 2020;2(9):3764-87.
- Shume WM, Murthy HCA, Zereffa EA. A Review on Synthesis and Characterization of Ag₂O Nanoparticles for Photocatalytic Applications. *Journal of Chemistry*. 2020;2020:1-15.
- Mardani HR, Forouzani M, Emami R. Efficient and green synthesis of trisubstituted imidazoles by magnetically nanocatalyst and microwave assisted. *Asian Journal of Green Chemistry*. 2019;3(4):525-35.
- Taghavi Fardood S, Ramazani A, Moradnia F, Afshari Z, Ganjkanlu S, Yekke Zare F. Green Synthesis of ZnO Nanoparticles via Sol-gel Method and Investigation of Its Application in Solvent-free Synthesis of 12-Aryltetrahydrobenzo[*a*]xanthene-11-one Derivatives Under Microwave Irradiation. *Chemical Methodologies*. 2019;3(6):632-42.
- Taghavi Fardood S, Moradnia F, Moradi S, Foroootan R, Yekke Zare F, Heidari M. Eco-friendly synthesis and characterization of α -Fe₂O₃ nanoparticles and study of their photocatalytic activity for degradation of Congo red dye. *Nanochemistry Research*. 2019;4(2):140-7.
- Taghavi Fardood S, Moradnia F, Mostafaei M, Afshari Z, Faramarzi V, Ganjkanlu S. Biosynthesis of MgFe₂O₄ magnetic nanoparticles and its application in photo-degradation of malachite green dye and kinetic study. *Nanochemistry Research*. 2019;4(1):86-93.
- Murthy HA, Abebe B, Prakash C, Shantaveerayya K. A review on green synthesis of Cu and CuO nanomaterials for multifunctional applications. *Material Science Research India*. 2018;15(3):279-95.
- Kumar MRA, Abebe B, Nagaswarupa HP, Murthy HCA, Ravikumar CR, Sabir FK. Enhanced photocatalytic and electrochemical performance of TiO₂-Fe₂O₃ nanocomposite: Its applications in dye decolorization and as supercapacitors. *Scientific Reports*. 2020;10(1).
- Abebe B, Murthy HCA, Zereffa EA, Adimasu Y. Synthesis and characterization of ZnO/PVA nanocomposites for antibacterial and electrochemical applications. *Inorganic and Nano-Metal Chemistry*. 2020:1-12.
- Azarbani F, Shiravand S. Green synthesis of silver nanoparticles by *Ferulago macrocarpa* flowers extract

- and their antibacterial, antifungal and toxic effects. *Green Chemistry Letters and Reviews*. 2020;13(1):41-9.
23. Huang W, Yan M, Duan H, Bi Y, Cheng X, Yu H. Synergistic Antifungal Activity of Green Synthesized Silver Nanoparticles and Epoxiconazole against *Setosphaeria turcica*. *Journal of Nanomaterials*. 2020;2020:1-7.
 24. Girón-Vázquez NG, Gómez-Gutiérrez CM, Soto-Robles CA, Nava O, Lugo-Medina E, Castrejón-Sánchez VH, et al. Study of the effect of *Persea americana* seed in the green synthesis of silver nanoparticles and their antimicrobial properties. *Results in Physics*. 2019;13:102142.
 25. Taghavi Fardood S, Forootan R, Moradnia F, Afshari Z, Ramazani A. Green synthesis, characterization, and photocatalytic activity of cobalt chromite spinel nanoparticles. *Materials Research Express*. 2020;7(1):015086.
 26. Moradnia F, Taghavi Fardood S, Ramazani A, Gupta VK. Green synthesis of recyclable MgFeCrO₄ spinel nanoparticles for rapid photodegradation of direct black 122 dye. *Journal of Photochemistry and Photobiology A: Chemistry*. 2020;392:112433.
 27. Sadeghi B, Gholamhoseinpoor F. A study on the stability and green synthesis of silver nanoparticles using *Ziziphora tenuior* (Zt) extract at room temperature. *Spectrochimica Acta Part A: Molecular and Biomolecular Spectroscopy*. 2015;134:310-5.
 - [28] Taghavi Fardood S, Moradnia F, Ghalaihi AH, Danesh Pajouh S, Heidari M. Facile green synthesis and characterization of zinc oxide nanoparticles using tragacanth gel: investigation of their photocatalytic performance for dye degradation under visible light irradiation. *Nanochemistry Research*. 2020;5(1):69-76.
 29. Mat Yusuf SNA, Che Mood CNA, Ahmad NH, Sandai D, Lee CK, Lim V. Optimization of biogenic synthesis of silver nanoparticles from flavonoid-rich *Clinacanthus nutans* leaf and stem aqueous extracts. *Royal Society Open Science*. 2020;7(7):200065.
 30. Velgosová O, Mražíková A, Veselovský L, Willner J, Fornalczyk A. Influence of Different Plants Extracts on Silver Nanoparticles Green Synthesis. *Archives of Metallurgy and Materials*. 2019;vol. 64(No 2):665-70.
 - [31] Ghotekar S, Pansambal S, Pagar K, Pardeshi O, Oza R. Synthesis of CeVO₄ nanoparticles using sol-gel auto combustion method and their antifungal activity. *Nanochemistry Research*. 2018;3(2):189-96.
 32. Marassi V, Di Cristo L, Smith SGJ, Ortelli S, Blosi M, Costa AL, et al. Silver nanoparticles as a medical device in healthcare settings: a five-step approach for candidate screening of coating agents. *Royal Society Open Science*. 2018;5(1):171113.
 33. Dhand V, Soumya L, Bharadwaj S, Chakra S, Bhatt D, Sreedhar B. Green synthesis of silver nanoparticles using *Coffea arabica* seed extract and its antibacterial activity. *Materials Science and Engineering: C*. 2016;58:36-43.
 34. Hu D, Ogawa K, Kajiyama M, Enomae T. Characterization of self-assembled silver nanoparticle ink based on nanoemulsion method. *Royal Society Open Science*. 2020;7(5):200296.
 35. Murthy HCA, Desalegn Zeleke T, Ravikumar CR, Anil Kumar MR, Nagaswarupa HP. Electrochemical properties of biogenic silver nanoparticles synthesized using *Hagenia abyssinica* (Brace) JF. Gmel. medicinal plant leaf extract. *Materials Research Express*. 2020;7(5):055016.
 36. Abebe B, Murthy HCA, Amare E. Enhancing the photocatalytic efficiency of ZnO: Defects, heterojunction, and optimization. *Environmental Nanotechnology, Monitoring & Management*. 2020;14:100336.
 37. Anbu P, Gopinath SCB, Yun HS, Lee C-G. Temperature-dependent green biosynthesis and characterization of silver nanoparticles using balloon flower plants and their antibacterial potential. *Journal of Molecular Structure*. 2019;1177:302-9.
 38. Thangamani N, Bhuvaneshwari N. Green synthesis of gold nanoparticles using *Simarouba glauca* leaf extract and their biological activity of micro-organism. *Chemical Physics Letters*. 2019;732:136587.
 39. Muthuvel A, Jothibas M, Manoharan C. Synthesis of copper oxide nanoparticles by chemical and biogenic methods: photocatalytic degradation and in vitro antioxidant activity. *Nanotechnology for Environmental Engineering*. 2020;5(2).
 40. Phull A-R, Abbas Q, Ali A, Raza H, Kim SJ, Zia M, et al. Antioxidant, cytotoxic and antimicrobial activities of green synthesized silver nanoparticles from crude extract of *Bergenia ciliata*. *Future Journal of Pharmaceutical Sciences*. 2016;2(1):31-6.
 41. Zhang H, Huang Y, Gu J, Keller A, Qin Y, Bian Y, et al. Single particle ICP-MS and GC-MS provide a new insight into the formation mechanisms during the green synthesis of AgNPs. *New Journal of Chemistry*. 2019;43(9):3946-55.
 42. Salmen SH, Alharbi SA. Silver nanoparticles synthesized biogenically from *Aloe fleurentinorum* extract: characterization and antibacterial activity. *Green Chemistry Letters and Reviews*. 2020;13(1):1-5.
 43. Abdel-Aziz MS, Shaheen MS, El-Nekeety AA, Abdel-Wahhab MA. Antioxidant and antibacterial activity of silver nanoparticles biosynthesized using *Chenopodium murale* leaf extract. *Journal of Saudi Chemical Society*. 2014;18(4):356-63.
 44. Jain S, Mehata MS. Medicinal Plant Leaf Extract and Pure Flavonoid Mediated Green Synthesis of Silver Nanoparticles and their Enhanced Antibacterial Property. *Scientific Reports*. 2017;7(1).
 45. Ghotekar S, Pansambal S, Pawar SP, Pagar T, Oza R, Bangale S. Biological activities of biogenically synthesized fluorescent silver nanoparticles using *Acanthospermum hispidum* leaves extract. *SN Applied Sciences*. 2019;1(11).
 46. Ibrahim HMM. Green synthesis and characterization of silver nanoparticles using banana peel extract and their antimicrobial activity against representative microorganisms. *Journal of Radiation Research and Applied Sciences*. 2015;8(3):265-75.
 47. Ghaedi M, Yousefinejad M, Safarpour M, Khafri HZ, Purkait MK. *Rosmarinus officinalis* leaf extract mediated green synthesis of silver nanoparticles and investigation of its antimicrobial properties. *Journal of Industrial and Engineering Chemistry*. 2015;31:167-72.
 48. Ayinde WB, Gitari MW, Muchindu M, Samie A. Biosynthesis of Ultrasonically Modified Ag-MgO Nanocomposite and Its Potential for Antimicrobial Activity. *Journal of Nanotechnology*. 2018;2018:1-10.